IEEE Access
Multidisciplinary | Rapid Review | Open Access Journal

Received June 3, 2018, accepted July 23, 2018, date of publication July 31, 2018, date of current version September 5, 2018.

Digital Object Identifier 10.1109/ACCESS.2018.2861572

Safety Tracking Motion Control Based on Forbidden Virtual Fixtures in Robot Assisted Nasal Surgery

QINGWEN ZHENG[1,2,3], YUCHENG HE[2,3], XIAOZHI QI[2,3], PENG ZHANG[2,3], YING HU[2,3], (Member, IEEE), AND BING LI[1], (Senior Member, IEEE)

[1]Harbin Institute of Technology, Shenzhen 518052, China
[2]CAS Key Laboratory of Human-Machine Intelligence-Synergy Systems, Shenzhen Institutes of Advanced Technology, Chinese Academy of Sciences, Shenzhen 518055, China
[3]Shenzhen Key Laboratory of Minimally Invasive Surgical Robotics and System, Shenzhen Institutes of Advanced Technology, Chinese Academy of Sciences, Shenzhen 518055, China

Corresponding authors: Xiaozhi Qi (xz.qi@siat.ac.cn) and Ying Hu (ying.hu@siat.ac.cn)

This work was supported in part by the National Natural Science Foundation of China under Grant U1613224, Grant U1713221, and Grant 61603374, in part by the Shenzhen Fundamental Research Funds under Grant JCYJ20160608153218487 and Grant JCYJ20170413104438332, in part by the China Postdoctoral Science Foundation under Grant 2018M631003, and in part by the Shenzhen Key Laboratory Project under Grant ZDSYS201707271637577.

ABSTRACT Traditional nasal surgery requires the doctor's left hand to carry the endoscope and right hand to complete the surgical operation using unstable images, potentially leading to danger due to mental fatigue, which may greatly prolong the operation time. Previously, robots in robot assisted endoscope sinus surgery (RAESS) only used simple linear motion control, lacked a dynamic tracking mechanism, and had no effective safety protection constraints, such as virtual fixtures or real-time force sensors. This paper describes an innovative and secure robotic control strategy for a dynamic automatic tracking endoscope with doctor input based on the mixed constraint of a dual-layer hyperboloid virtual fixture generated by a series of key points around the nasal cavity and a model of the threshold contact force. A tracking control strategy is set up after calibrating the navigation system and motion filtering via a human-machine interaction. Several experiments show that the hyperboloid virtual fixtures can generate an efficient constraint of different robotic motions and that the robot can automatically execute a track mission with high precision. The proposed safety protection method can be easily applied to patients with different nose shapes and greatly improve the quality of surgery.

INDEX TERMS Robot assisted nasal surgery, virtual fixtures, automatic tracking control, security control strategy.

I. INTRODUCTION

Chronic sinusitis is an acute suppurative inflammation of the mucous membrane of the sinuses, which has affected as many as 300 million; the number of deaths caused by nasal cancer increases every year. Open surgery was the first type of surgery in the sino-nasal area. Wigand [1] and Messerklinger [2] pioneered the use of the endoscope to perform nasal surgery and treat the related functional disease. *Functional Endoscopic Sinus Surgery* (FESS) combined with endoscope imaging technology is the most effective method of treating nasal disease. In endoscopic surgeries, a right-handed surgeon stands at the side of the patient carrying the surgical instrument used to aspirate soft tissue fragments and opens different structures using their right hand, while holding the endoscope with their left hand. This type of surgery means that the surgeon has to carry the endoscope, resulting in frequent switching of instruments from hand to hand; as a result, unsteady endoscopic images and potential surgical risks caused by long-term holding fatigue and mental fatigue may greatly prolong the operation time. Coordination between doctors and assistants may cause problems, such as incomplete resection or goiter rupture. To overcome this difficulty and reduce the invasiveness and pain to the patient, a third hand holding the endoscope can liberate the surgeon's hands and switch the surgery to the ''two hand simultaneous operation'' mode to improve the quality and safety of the operation.

In previous studies, *Robot Assisted Endoscopic Sinus Surgery* (RAESS) reduced doctor tremors and improved their freedom of movement as well as led to flexible operation

modes, which greatly broadened the applications of *Minimally Invasive Surgery* (MIS). The Computer Motion company in the United States developed the mirror holding robot AESOP for minimally invasive surgery in 1994, which marked the beginning of RAESS [3], [4]. AESOP is able to control a celiac endoscope camera using voice instructions. Another master-slave remote control operation robot, ZEUS, was also designed, and its patient-side system, which contains a mechanical arm that holds an endoscope, makes it time-saving and effective [5], [6]. In the da Vinci robotic system, an endoscopic arm provides the same high-resolution images of the visual field as an open operation, while its instrument arm increases the flexibility of the operation; however, this system is not suitable for nasal surgery due to its large size and master-slave control model. Several endoscopic robots have been developed; the endoassist robot designed by the Armstrong company uses an infrared induction device and foot pedal to adjust the position of the endoscope up and down and enlarge and reduce endoscope vision [7], [8]. The Tiska endoarm system has an RCM mechanism that is based on a double parallelogram to obtain a stable position and pose and uses a foot pedal to control the locking and loosening of the joint. The Tx40 active robot endoscope system developed by Technical University of Braunschweig, which consists of a navigation system, tracking system and friendly human-computer interface, is considered to be the most integrated endoscopic surgery robot. Li *et al.* [9] developed a robotic system that has an arm with four *Degree Of Freedom* (DOF) and a wire-driven double parallelogram mechanism to control the pitching, rolling, yaw and insertion depth of the endoscope in the nasal cavity in a decoupled manner. In our previous work, a seven DOF endoscope holder was designed and a registration between the robot, CT image data and stereoscopic optical equipment was developed in addition to path planning using the A star algorithm [10], [11]. Among all of the introduced endoscopic robots, there are still some shortcomings and limitations. First, most of them use a simple linear motion control and lack a dynamic endoscope tracking mechanism. Also, there are no effective safety protection devices, such as virtual fixtures or real-time force sensors, for the narrow nasal space, and the systems are still inaccurate in their operation. Using a passive joint robot, which has a hydraulic or pneumatic locking mode, a surgeon needs to manually adjust the position and posture of the endoscope by frequently interrupting the operation. Finally, due to the limitations of the dynamic control methods, a fully automatic endoscopic robot has not been produced. To address these challenges, we established an innovative human-machine interaction implementation method to dynamically track endoscopic surgical instruments with as much autonomy as possible based on a space dynamic customizable virtual fixture constraint and safety control strategy. This method can provide stable endoscopic images with different surgeon hand movements using a motion tracking instrument and effectively protect the nasal cavity under the robotic space constraint and threshold force model.

Compared to position, velocity and acceleration constraints, the virtual fixture method is one of the most popular techniques to avoid collisions between surgical instruments and organs in the field of robot safety design and path planning. These techniques have been successful in assisting people to perform tasks faster and more accurately in surgery [12], [13] as well as in manufacturing applications. Different from *Guided Virtual Fixtures* (GVFs), which are used to guide operators to track the desired motion path, *Forbidden Virtual Fixtures* (FRVFs) can limit the movement of robot end effectors in a safety area. In MIS, there are several methods to build a virtual fixtures model. Li *et al.* [14] developed a spatial-motion-constraints approach by combining the user's force input with a planned tip-trajectory to create the tip motion constraints, which generates tool-shaft boundary constraints on a 3D rigid model reconstructed using CT data. Ren *et al.* [15] used preoperative dynamic *Magnetic Resonance* (MR) or *Computed Tomography* (CT) images to create dynamic *3D Virtual Fixtures* (DVFs) to provide the surgeon's hand with more guidance and protect sensitive structures by constraining the surgeon's hand motions. Wurm *et al.* [16] and Lueth's group [17]–[19] used CT data to generate a 3D virtual fixture, but it made the preoperative phase complex and time-consuming. Virtual fixtures were also created from sensor data. Ryden *et al.* [20] used haptic rendering of the stream point cloud captured from a Kinect camera to protect a beating heart to generate virtual fixtures. Park [12] proposed a sensor-based virtual fixture by restricting robot motion and providing tactile feedback, which was able to guide surgeons to move surgical instruments along the desired direction. Becker *et al.* [21] derived a control law for a position-based virtual fixture, which was generated in real-time from a microscope video. Selvaggio *et al.* [22] used computer vision as a sensor to generate an interactive system through online fixed virtual fixtures. These types of virtual fixtures suffer from several drawbacks, such as a limited field of view, occasional loss of signal, too small workspaces and, in some cases, interpretation difficulty. Use of a spatial geometric model or point clouds near organ tissue to build a virtual fixture has also been widely studied for use in adaptive applications, particularly in dynamic and unstructured environments. Nakazawa *et al.* [23] developed a truncated cone shaped virtual fixture that was generated by marking workspace edges without a force sensor or preoperative imaging data. Tang [24] marked critical areas near the surface of vulnerable organs before or even during surgery to generate virtual fixtures, which is low-cost and very easy to use. Fardel *et al.* [25] at TU Brauschweig used sensor data from a stereo camera system above the surgeon's workspace to track the position of the surgeon input, which lacks the dynamic space constraints of movements, such as virtual fixtures. In our work, to realize a robot security protection and innovative tracking mechanism for endoscopic sinus surgery, a hyperboloid was generated via a series of spatial points to build a virtual fixture to adapt to different nasal shapes; it is fast and easy-to-use compared to traditional methods.

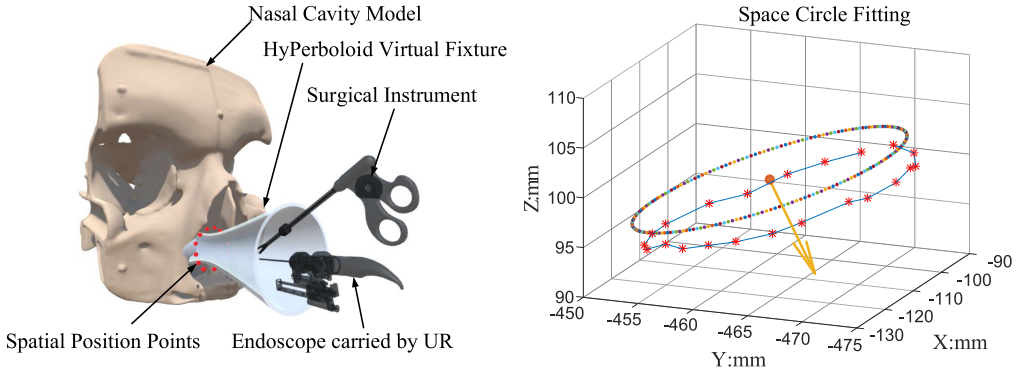

FIGURE 1. Spatial relationship between the instrument and endoscope and the generation process of the hyperboloid virtual fixtures and its spatial base circle fitting circle (centre of the circle and normal vector) by the Least Square Method, Lagrange Method and Square Difference Method. (a) Hyperboloid Virtual fixtures generated by spatial points. (b) Space circle fitting result.

Then, an automatic tracking strategy was developed based on the mixed constraints of virtual fixtures and the threshold force model.

This paper is organized as follows: the process of building virtual fixtures is discussed in Section II, the automatic tracking motion based on virtual fixtures is presented in Section III, and the security control strategy is described in Section IV. The experimental and results discussions are presented in Section V. Finally, conclusions and future work are presented in Section VI.

II. BUILDING PROCESS OF VIRTUAL FIXTURES

Most virtual fixtures are generated via accurate 3D human nasal cavity biological data models that are obtained using preoperative medical imaging systems, such as MRI or CT. Unlike this traditional, complex and time-consuming model, a new framework method, which is useful for different nasal shapes, is proposed without the need for 3D pathological area data. Under the "small entrance—large internal funnel-shaped space" nasal cavity structure, which has a narrow and crowded space, the robot holding the endoscope swings around the nostrils to avoid potential collisions and conflicts among the surgical instruments, endoscope and nasal tissue at any time during the surgical process. This means that a space virtual fixture can be automatically generated through a series of nasal accessory key points to construct the hyperbolic constraint model, as shown in Fig. 1 (a). Nasal endoscopic surgery allows the nostril to have a certain pull deformation, so that the instrument can reach the surgical site smoothly and therefore obtain more operation space. The experiment shows that this method is very effective in reducing the rate of surgical error and protecting the human body to a maximum degree.

A. CONSTRUCTION PROCESS OF THE HYPERBOLOID CONSTRAINT MODEL

The building process of hyperboloid virtual fixtures can be divided into the following steps under the consideration of a hyperboloid expression. The first step is to drive the Universal Robot 5, which has a terminal actuator at the end of the endoscope that is able to move around the entrance of the nasal cavity to record the spatial key point set; this set can be easily and precisely obtained and recorded via computer programming through *TCP/IP* communication with a 0.1 mm accuracy. Based on the series of points $(3 \times n)$ recorded as $X_i^3 = \{(x_1, \cdots, x_n)|i = 1, \cdots, n\}$, the fitting space circle O and its normal vector F can be generated by the fitting plane through the intersection of the space plane and sphere built by the Least Squares Method, Lagrange Method and Indirect Square Difference Method. The fitting result is shown in Fig. 1(b).

$$\begin{cases} \min\limits_{O,R} \sum\limits_{i=1}^{n} |\|O - X_i\| - R| = \min\limits_{O,R} \left(V^T P V\right) \\ X = \left(A^T P A\right)^{-1} A^T P L \\ \min\limits_{F} \left(F\left(O - X\right)\right)^2, \quad s,t.\ \|F\| = 1 \end{cases} \tag{1}$$

In the second step, three types of virtual fixtures aimed at endoscope end P carried by a UR robot are generated. The tractive deformability of the nasal cavity, which is described by a dual-layer-hyperboloid model that is defined by the ratio coefficient $k(0 < k < 1)$, with an inner layer is thought to be the safest area, and that with an outer layer is thought to be the dangerous area. The speed of the robot satisfied the constraint functions according to the degree of deviation.

The definition of the coefficient k, for example, in position constraint stands for the degree of deviation which can be calculated as ratio of the r_t and R_t as Fig. 2 shown. Therefore k_p, k_θ and k_E are the prescribed parameters which can be formulated according to different dual-hyperboloid design within the range of 0 and 1.

These constraints are shown in Table 1. Beyond the outer layers, a safety force sensor can be used to define the mix of the virtual constraint force and actual contact force, which can dynamically limit the current speed of the robot.

TABLE 1. Three types of robot constraints generated by hyperboloid virtual fixtures.

Constraint type	Parameters	Constraint condition	Robot speed	Figure illustration
Position constraint	Dis : distance between P and O . d : distance between P and the base plane. R : radius of the current circle. r : $r=\sqrt{Dis^2-d^2}$	$r \le R$	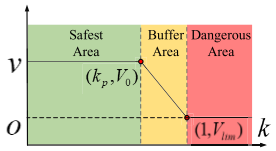	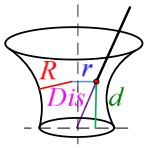
Orientation constraint	φ : angle between the endoscope line direction and normal vector. θ : asymptote angle defined by the hyperboloid parameter.	$\varphi \le \theta$	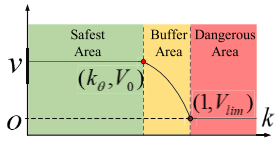	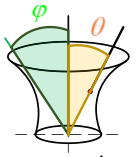
Endoscope axis-line direction constraint	d_0 : distance of intersection of the plane and O . R_0 : radius of the base circle.	$d_0 \le R_0$	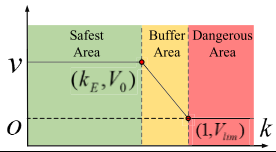	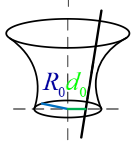

TABLE 2. Approximate threshold force in the nasal cavity.

Open Sinuses(N)				Maximum Contact/Deformation Force(N)						
front	ethmoidal	maxillary	sphenoid	vestibule	soft-tissue	bone-tissue	mucosa	I.turbinate	M.turbinate	S.turbinate
2-12	8-26	4-10	6-22	9.7885	8.4384	10.2845	3.5628	8.4384	7.0300	5.6245

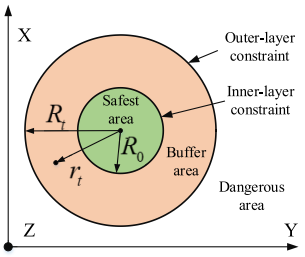

FIGURE 2. Cross section of Dual-layer-hyperboloid constraint model.

B. ROBOTIC MIXED CONSTRAINTS MODEL

In RAESS, the shape, topological structure and geometric size of an endoscope should comply with the kinematics of a human arm and should cooperate well with a surgeon's hand movements during the procedure. In a cluttered environment, such as an *Operating Room* (OR), an endoscope has to be safe for both surgeon and patient and as compact as possible. To quantify these specifications, the characteristics of the contact mechanics of different nasal tissues, especially the key tissues related to operative safety, such as mucosal tissue be able to overcome when traversing the sino-nasal tract. A 6-axis Force-Torque (FT20331) sensor (Nano 43, ATI, American) is mounted on the endoscope (Fig. 3) to completely open all of the sinuses (frontal sinus, sphenoid sinus and ethmoid sinus) as deeply as possible. The endoscope and surgical instrument are sufficiently rigid to work without excessive bending. Table 2 shows the endoscope and surgical instrument are sufficiently rigid to work without excessive bending. Table 2 shows the approximate threshold forces to prevent the robot from injuring the human nasal cavity. These forces are not sufficient to contribute to the biomechanics; however, they are necessary and sufficient to control the robot's automatic tracking motion with the help of the virtual fixture. Table 2 shows ATI sensor data after initializing the natural offset by applying a known load in a known direction (in our case, the handle weight along the z axis). The maximum contact or deformation force is calculated by the resultant force of the axial viscous force and radial pressure force data, which is within the range of the threshold force.

A contact force-based safety speed V_s is set up so that if the robotic contacting force reaches a maximum, the robot would stop. This constraints method, which is based on the feedback of the back force sensing signals, is not suitable when the doctor opens some sinuses. In conclusion, two types of speed functions are used in the linear equation and curvilinear equation, in which k stands for the degree of deviation mentioned above, as shown below:

$$f(v_1) = \begin{cases} V_0, & k \le k_1 \\ \dfrac{V_0 - V_{lim}}{k_1 - k_2}(k - k_1) + V_0, & k_1 < k < k_2 \\ V_{lim}, & k \ge k_2 \end{cases} \quad (2)$$

$$f(v_2) = \begin{cases} V_0, & k \le k_1 \\ \dfrac{V_{lim} - V_0}{(k_1 - k_2)^2}\left(k^2 - 2k_1k + k_1^2\right) + V_0, & k_1 < k < k_2 \\ V_{lim}, & k \ge k_2 \end{cases} \quad (3)$$

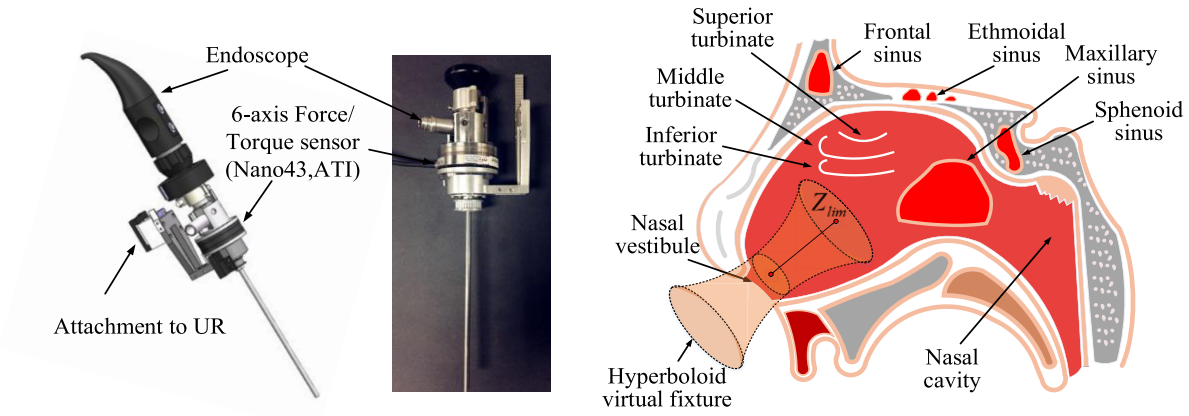

(a) (b)

FIGURE 3. Sketch map of the nasal cavity and suitable hyperboloid in this "funnel" shaped cavity; the threshold Z_{lim} is set and limits the height of the hyperboloid so that in the narrow and complex nasal cavity, spatial constraints are only effective within the scope of validity. (a) ATI sensor installation position. (b) Sketch of the nasal cavity and the position of the virtual fixture.

The mixed virtual fixture algorithm is shown below:

Algorithm 1 Hyperboloid Mixed-Contact Constraint Model

Initialize:

Robot end-effector registration and ATI force sensor installation

Collect X_i^3, calculate $O(x_0, y_0, z_0)$, normal vector μ_H

Threshold force data model

Set ratio k_1, k_2, K_s and V_o, V_{lim}, V_S

While true:

if $f_t < \varepsilon_L$:

if $r_t \le k_1 R_t$ && $\varphi_E \le k_1 \theta_H$ && $d_{o,t} \le k_1 R_o$

Robot free move with $v = V_o$

else if $k_1 R_t < r_t \le k_2 R_t$ && $k_1 \theta_H < \varphi_E \le k_2 \theta_H$ && $k_1 R_o < d_{o,t} \le k_2 R_o$

Robot $v = f(v_1)$ or $v = f(v_2)$

else if $r_t > k_2 R_t$ && $\varphi_E > k_2 \theta_H$ && $d_{o,t} > k_2 R_o$

Robot $v = V_{lim}$

else if $\varepsilon_L \le f_t < \varepsilon_H$:

Robot $v = V_S$

else if $f_t \ge \varepsilon_H$:

Stop robot

if the operation is done or close the virtual fixture:

break

end while

III. AUTOMATIC TRACKING STRATEGY BASED ON VFS

To achieve robotic tracking of the input from the doctor's hand, which is more flexible and intelligent than a robot operating at a predetermined trajectory, a robotic dynamic tracking strategy is developed that has high tracking accuracy and security due to the protection of the mixed constraints model, as well as a good human-machine interaction design. During the operation, a piecewise exponential function that allows the end of the endoscope to dynamically follow the instruments is built according to the spatial relationship between the endoscopic end and the tip of the surgical instrument, and its position is always on the sphere formed by the instrument.

Through an external tracking method, the position, posture, velocity and acceleration parameters of the instruments held by a surgeon are acquired in real time after filtering.

A. CALIBRATION PROCESS OF THE NAVIGATION SYSTEM

The basis for tracking motion is to install the target information on surgical instruments to obtain inputs from the instruments carried by doctors. A three-dimensional optical positioning instrument device (Polaris Vicra, NDI, Canada) is used by our program, which uses OAPI to custom-write C++ code and is integrated into the overall control system to continuously stream the Optotrak sensor data to the PC. However, the spatial motion of surgical instruments measured by NDI is based on the Descartes coordinate system, which needs to be calibrated into the robotic coordinate system. Thus, a 3D point cloud registration process based on a robot to find a 4*4 transformation matrix is proposed to obtain the relation between NDI points and UR points, which is a one-to-one mapping relation, to find the nearest points to match them. The corresponding set of points N (NDI measurements) and U (UR measurements) can be constructed directly, as follows:

$$N = \{N_i\} \in R^3, \quad U = \{U_i\} \in R^3, \ i = 1, 2, 3, \cdots, N \tag{4}$$

Then, by finding the registration conversion, the relation of the single point transformation is:

$$\hat{U}_i = R_{3\times3} \cdot \hat{N}_i + T_{3\times1}, \quad i = 1, 2, 3, \cdots, N \tag{5}$$

R is a 3*3 rotation matrix, and T is a translation vector. Therefore, the rigid transformation between point clouds can be constructed as $q = [R|T]$, which minimizes the error function:

$$f(q) = \frac{1}{N_P} \sum_{i=1}^{N_P} \| U_i - (R \cdot N_i + T) \|^2 \tag{6}$$

Next, the translation vector T is estimated and removed by translating N and U to their centroid n and u, respectively:

$$\begin{cases} n = \frac{1}{N_P}\sum_{i=1}^{N_P} N_i, u = \frac{1}{N_P}\sum_{i=1}^{N_P} U_i \\ n_i = N_i - n, u = U_i - u \end{cases} \quad (7)$$

Therefore, the above optimization objective function can be converted as:

$$E = \sum_{i=1}^{N_P} \|u_i - R \cdot n_i\|^2 = \sum_{i=1}^{N_P} (u_i^T u_i + n_i^T n_i - 2RG) \quad (8)$$

Then, using singular value decomposition of G, the smallest E can be obtained as well as the R and T matrix:

$$\begin{aligned} [U, S, V] &= SVD(G) \\ R &= VU^T \\ T &= -R \cdot n + u \end{aligned} \quad (9)$$

In our program, the transformation matrix T can be generated as follows:

$$T_{NDItoUR} = \begin{bmatrix} R_{00} & R_{01} & R_{02} & T_{00} \\ R_{01} & R_{11} & R_{12} & T_{01} \\ R_{02} & R_{12} & R_{22} & T_{02} \\ 0 & 0 & 0 & 1 \end{bmatrix} \quad (10)$$

Above all, any surgical instrument movements can be converted into the robotic coordinate system within the range of the NDI observation. However, this transformation matrix is not suitable for robot pose tracking. Therefore, using NDI to obtain the quaternion of Optical target1, with its transformation matrix set as T_{N1}, the rotation matrix T_{NtoU} between the UR robot and target1 can be easily obtained; thus, the relation between the UR robot and NDI system can be derived as $T_{URtoNDI}$. Finally, by installing the Optical target2 (T_{N2}) at the surgical instrument, its orientation can be obtained, which is expressed as:

$$\begin{aligned} T_{URtoNDI} &= T_{N1} \cdot T_{NtoR} \\ T_{tracking} &= T_{N2} \cdot T_{URtoNDI}^{-1} = T_{N2} \cdot T_{NtoR}^{-1} \cdot T_{N1}^{-1} \end{aligned} \quad (11)$$

B. MOVEMENT STRATEGY AND PLANNING ANALYSIS

After the calibration of UR and NDI is conducted, the expected position is sent to the UR robot, designed by a high precision PD position control at a fixed refresh frequency of 100Hz to set up the tracking movement strategy. To give the doctor the best surgical angle and a clear and smooth visual field, the relationship model between the nasal endoscopy tip and instrument end in the doctor's hands must be established, as shown in Fig. 4. Nine tracking strategies built by angle and distance are generated on the safety area to ensure that the tip of the endoscope will always follow the end of the surgical instrument and remain dynamically at the sphere centred on the end of the surgical instrument with a certain radius and at certain angles, as shown in Table 3.

However, any small tremor of the doctor's hand may cause unnecessary vibration of the robot leading to high-frequency noise, and a wide range of surgical instrument movements will cause the robot to run at a dangerously high speed. Therefore, a "band-pass" filter for the operation of surgical instruments to avoid shaking and limit the robot's speed is proposed by recording the distance information $D_{I,t}$, which is between the current position $P_{I,t}$ and last moment position $P_{I,t-1}$ of the surgical instrument. Denoted as $D_{I,t} = \left\|\overrightarrow{P_{I,t}} - \overrightarrow{P_{I,t-1}}\right\|$, the threshold $\varepsilon_{DL}, \varepsilon_{DH}$ is set up such that if $\varepsilon_{DL} < D_{I,t} < \varepsilon_{DH}$, the robot will continue its tracking motion; otherwise, it will hover at $P_{I,t-1}$ until the range of the hand movements increases.

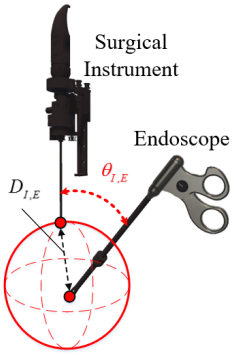

FIGURE 4. Spatial relationship between the instrument and endoscope.

There is a certain error in the registration method that can be fixed by manually adjusting the TCP of the robot to set the most accurate $D_{I,E}$ and $\theta_{I,E}$, as provided in Table 3.

TABLE 3. Most suitable distances and angles.

$D_{I,E}\,(mm)$	$\theta_{I,E}\,(\circ)$
5	30
10	45
15	60

In the tracking strategy, due to the uncertainty of the model parameters, to achieve more accurate acceleration tracking, real-time surgical instrument motion information can be obtained by an axis acceleration sensor module. The module can measure the three-axis rotation angle velocity and three-axis acceleration with 200Hz frequency and 0.01g precision of error in its Cartesian coordinate system. In surgery, the distance between the sensor and PC is so short that by using Bluetooth communication to access the acceleration sensor information from an Arduino UNO Microcontroller, the signal can be transmitted to the robot control program through serial port communication. Wireless communication can also reduce the interference to the doctor. To eliminate the interference of acceleration noise, an adaptive Kalman filter is used to filter out impurity mutation information, as shown in Fig. 5. After smoothing the signal, the fitting result makes the acceleration changes smoother and more continuous.

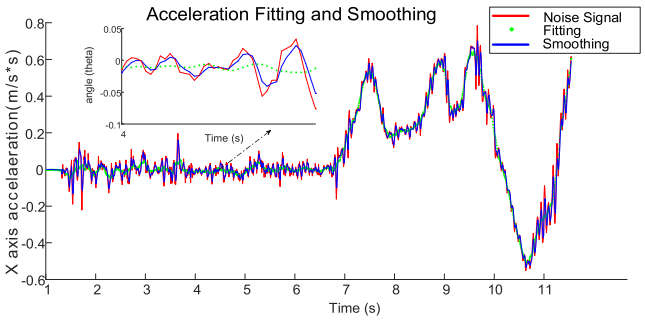

FIGURE 5. X-axis acceleration after an adaptive Kalman filter.

C. HUMAN-MACHINE INTERACTION AND ROBOT CONTROL

In the field of surgical robotics, a well-designed human-machine cooperative control strategy can not only lead to high precision and quick response of the robot but also relies on clinical experience and subjective control to ensure that the operation process is high quality safe; a well-designed strategy can also improve the doctor's operation experience. In our previous research, a 7 DOF robotic endoscope holder was fully controlled by a foot-attached IMU sensor with complicated operation and low operation precision. In our work, by using the design of a foot pedal human-computer interaction model, the automatic cleaning lens control can be set, which guides the robot to follow a secure predetermined path and clean the lens at the designed flume with no need for injecting salt water or even removing surgical instruments from the nose. Hovering or tracking controls are via the left foot pedal to achieve the "Follow - Temporarily hover - Follow" mode, while the automatic cleaning lens can controlled by the right foot pedal. Therefore, the control block diagram of the tracking motion based on the human-computer interaction is shown as follows:

Algorithm 2 Tracking Motion Control Algorithm

Initialize:
NDI: $P_I\ (x, y, z)$;
Coordinate Registration;
Robot Mixed Constraints Model;
While true:
if the foot pedal is pressed down:
If the left foot pedal is pressed down:
Automatic clean lens;
Else if:
Track surgical instruments (with filtering);
Else:
Temporarily hover;
if the operation is done or close the mixed constraints model:
Break
end while

The whole control system is implemented on a PC with a core i7 processor and 8GB of RAM. The C++ language

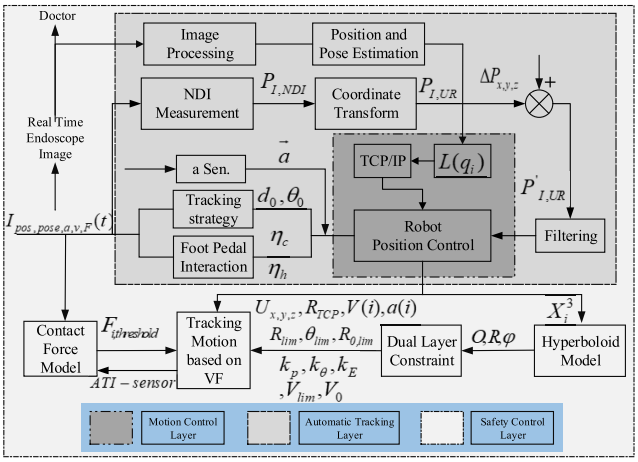

FIGURE 6. Three-layer safety control framework.

is used to generate the robot control software based on the QT platform shown in Fig. 6. Various robot current states and control instructions to the UR robot are transferred through the TCP/IP protocol and the hyperbolic constraint model, and the following automatic strategy is constructed based on the built software system.

IV. ROBOT SAFETY CONTROL

In nasal endoscopic surgery, taking into consideration the safety of the movement of the robot from the view of the doctor, it is necessary to construct a three-layer safety control framework, which is generated by a robot motion control layer, automatic tracking layer and safety monitoring layer to establish the human-machine security RAESS control model shown in Fig. 6.

First, the robot control layer is generated, and the UR robot converts the joint angle to the end-effector space position through forward kinematics and PID control, the and robot current states are transmitted through TCP/IP communication to the PC.

Then, at the automatic tracking layer, the input from the surgeon's hand $I(t)$ includes the position, pose, speed, acceleration of the instruments and the contact force with nasal tissue. The instrument $I(t)$, through an NDI measurement as $P_{I,NDI}$ and a transformed coordinate as $P_{I,UR}$ after TCP position compensation as ΔP, can filter out the unsteady-image influence of hand-shaking to obtain the tracking target. On the other hand, the three-dimensional acceleration $I(t)$ can be measured and filtered with the Kalman filter; three tracking strategies have been formulated to define the d_0, θ_0 applied to different operation tasks. The human-machine interaction based on the foot board can control the robot's automatic cleaning (η_c) of the lens and the instruction to hover at a certain position (η_h). In the future, endoscopic image processing to generate more accurate motion tracking by a visual servo system will also be considered. At the outermost security monitoring layer, it is necessary to consider the contact force $F_{i,threshold}$ because our flexible virtual fixture is built

by simplifying the nasal space. If the force does not exceed the threshold, the designed virtual fixtures can be used to constrain the speed of the robot. The parameters O, R, φ can be used to generate the dual layer constraint and limit tracking motion based on the parameters $R_{lim}, \theta_{lim}, R_{0,lim}, V_{lim}, V_0$ and robot states $P_{x,y,z}, R_{TCP}$. In the model, setting the threshold of hyperboloid can constrain the robot in the scope of validity, and for a deeper space, the real-time force sensor is used to make the decision of whether the robot should continue to move. This hierarchical control plays a different role in different tasks and can also cooperate to control the motion of the robot at the same time to achieve intelligent control of the tracking motion.

V. EXPERIMENTS AND ANALYSIS

A. EXPERIMENTAL IMPLEMENTS

The experimental setup is configured on the RAESS system, as shown in Fig. 7. A 4*4 coordinate transform matrix is obtained via the calibration process between UR and NDI, and a series of spatial key points is collected by the endoscope end held by the UR robot is used to build the virtual fixture. For the experiments, by placing the PHACON skull simulation model (Germany) under the view of an endoscope carried by the UR installed with NDI optical targets, real-time nasal cavity images with a cold light source via the imaging system can be received to judge the stability and effectiveness of the motion tracking controlled by the control software.

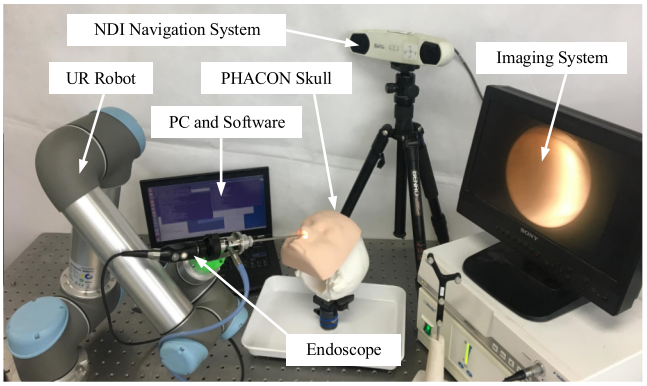

FIGURE 7. Experimental set up containing a software control system generated by the Qt platform based on the C++ language and hardware with an endoscope imaging system and cold-light source.

B. VIRTUAL FIXTURES CERTIFICATION

To verify the validity of the hyperbolic model and the constraint of the mixed constructed model, in the process of building a space circular plane through a set of space points, the circle centre point $O_H(x_0, y_0, z_0)$, circle radius R and normal vector $\mu_H(\mu_x, \mu_y, \mu_z)$ of the plane are obtained by the least squares method and the Lagrange equation. The residuals of plane fitting can be represented by the distance from the measured points to the fitting plane, while the residuals of the fitting circle can be represented by the difference between the distance from the measured points and radius R. Adjusting the fitting circle in offline CT data or generating it by driving the robot along a specific special circular object can improve the acquisition precision. This construction method is accurate and effective. In the hyperbolic model, the trajectory of the endoscope is recorded by completing specific tracking motions and analysing the effects of the constraints; this experiment does not consider the dynamic contact force between the endoscope, and nasal tissue, which is only considered to verify the validity of the modified model. First, verification of the dual-layer hyperboloid model by designing different hyperboloid shapes is performed by adjusting different model parameters (a, b, c) and analysing the speed changes of the robot. The shape of our fitting shape of the nasal cavity entry is a space circle, so we set $a = b = R_0$ in the model. Verification of the degree of inclination of the hyperboloid, which corresponds to the asymptote angle, can constrain the axial direction of the endoscope carried by the UR to verify the model.

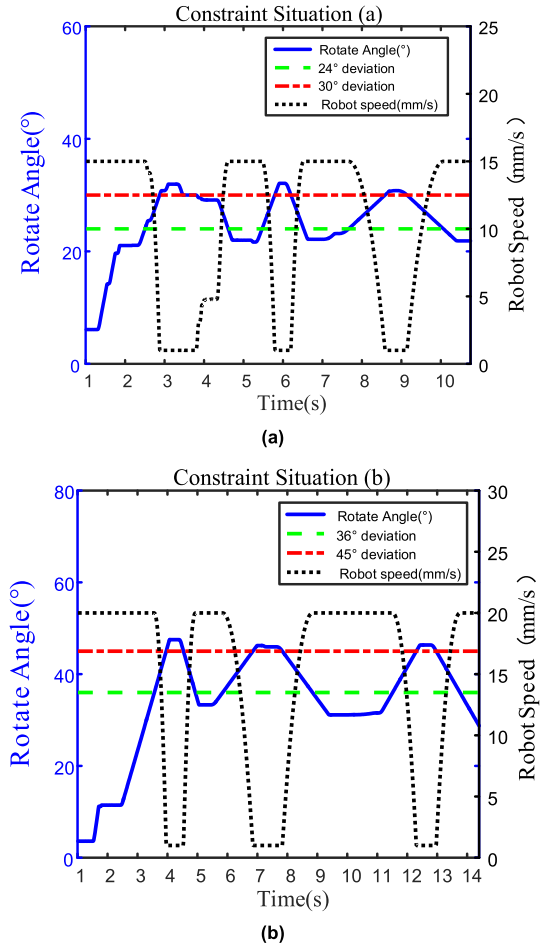

FIGURE 8. The blue lines represent the deviation angle between the endoscope line and normal vector; the red dotted lines represent the maximum allowable angle of the outer layer, while the green lines represent the inner angle. The black dotted lines represent the robot speed. The speed of the robot satisfies the angle constraint of the virtual fixtures algorithm. (a) $\theta_{outer,max} = 30^0$, $V_{lim} = 1mm/s$, $V_0 = 15mm/s$. (b) $\theta_{outer,max} = 45^0$, $V_{lim} = 1mm/s$, $V_0 = 20mm/s$.

Two types of angle constraints, which are shown in Fig. 8, are generated:

After verifying the adjustability and validity of the hyperboloid, the corresponding constraints for different robotic spatial positions and endoscope postures and their results still need to be verified.

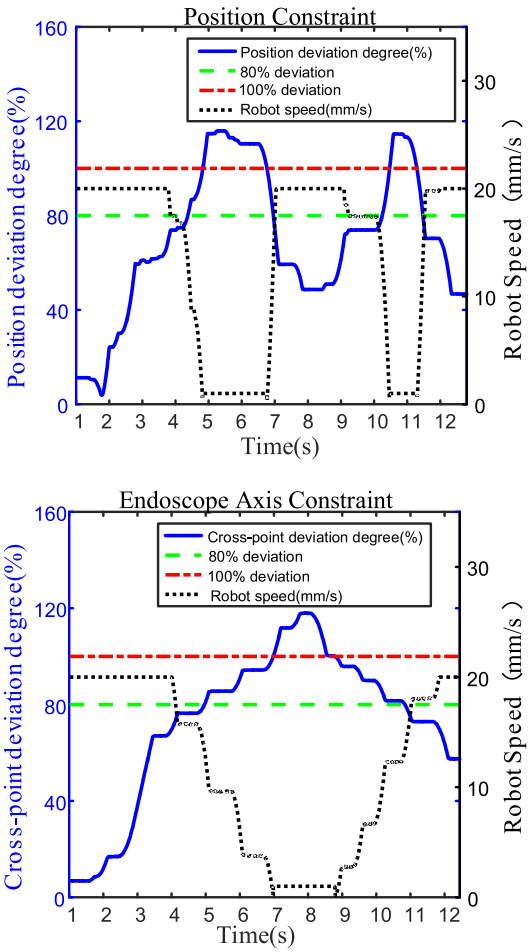

FIGURE 9. The blue lines represent the deviation angle between the endoscope line and normal vector; red dotted lines represent the maximum allowable angle of the outer layer, while the green lines represent the inner angle. The black dotted lines represent the robot speed. The speed of the robot satisfies the angle constraint of the virtual fixtures algorithm.

The experimental results of the position constraint of the robot by virtual fixtures is shown in Fig. 9. The blue line represents the distance ratio φ between the distance r_t of the current endoscope end position to the centre of the circle and the radius of the circle R_t. If $\varphi \leq 80\%$, the robot moves with $V_{lim} = 20mm/s$; if $80\% < \varphi \leq 100\%$, the speed of the robot has a linearly decreasing relationship with φ; otherwise, the robot moves with $V_0 = 1mm/s$. The experimental results show that the proposed algorithm effectively constrains the speed of the robot for different spatial positions. For the same situation, the axial constraint of the endoscope is the same as the position constraint, where the blue line represents the distance ratio γ, which is the distance d_0 between the cross point of the endoscope and the base circle to the centre of the base circle and the radius R_0 of the circle.

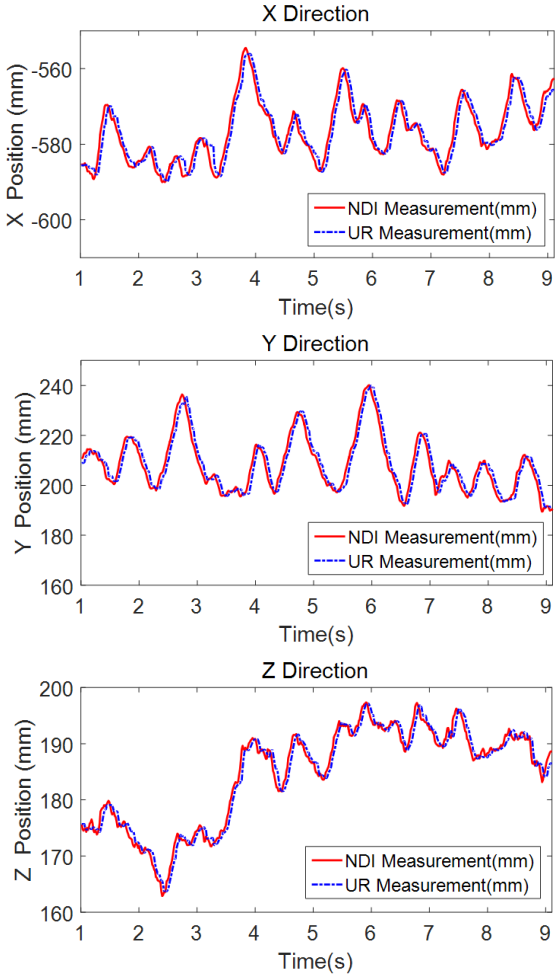

FIGURE 10. Position tracking and error in the X, Y, and Z directions: In the tracking stage, the robot conducts unconstrained tracking of the instrument when the foot pedal is pressed down. In the operation stage, if the pedals are lifted, the robot will hover at the final tracking posture. During all stages, if the NDI navigation signal is lost, the robot will remain still.

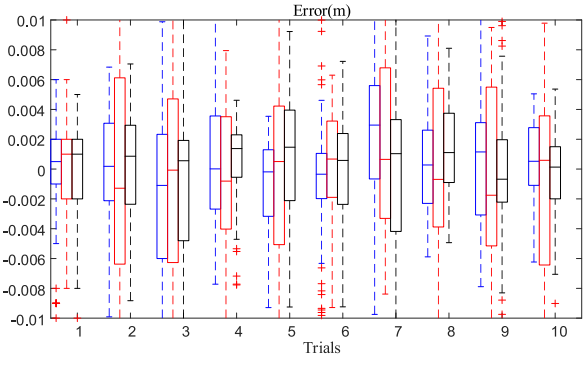

FIGURE 11. Ten groups of experiments to verify the effectiveness of the registration algorithm. The median is approximately 0 mm to 1 mm, while the upper and lower quartiles are all near at 2 mm to 4 mm in the X, Y, and Z directions in 10 experiments. Abnormal values are excluded due to the loss data of NDI navigation.

C. TRACKING MOTION BASED ON VFS VERIFICATION

This experiment is performed to evaluate the performance and effectiveness of the robot tracking of the surgeon's input,

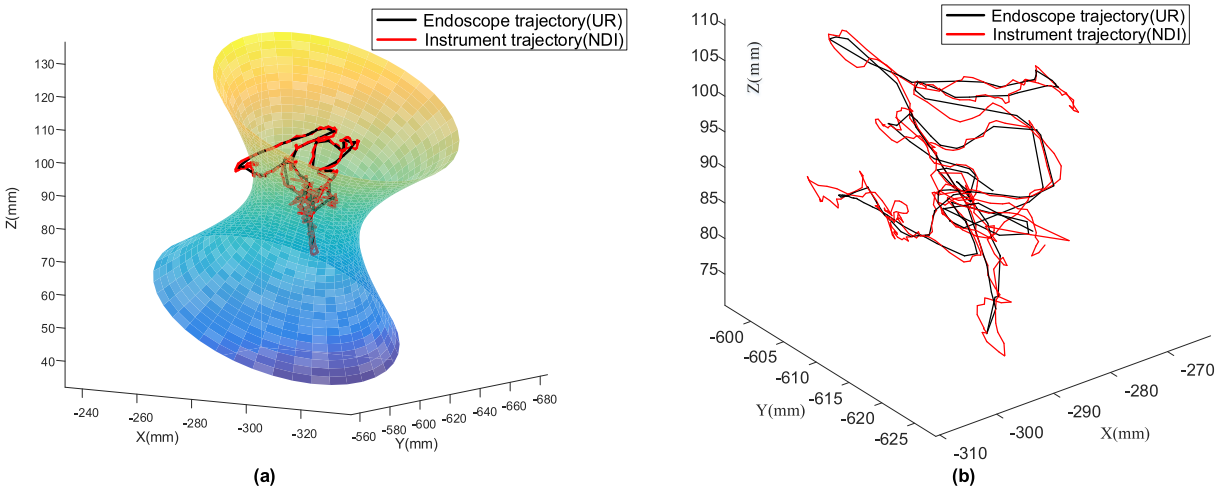

FIGURE 12. When instrument tracking at the outermost position constraint layers, the robot speed slows to 1 mm/s, and we change the move direction of the instrument so that the robot moves back into the hyper-circle and its speed reaches 20 mm/s. (a) Visualization of the spatial trajectories of the endoscope and surgical instrument under the hyperboloid model. (b) Trajectory of the 3D spatial tracking motion of the endoscope and the instrument carried by doctors.

TABLE 4. Errors of tracking motion.

Error	Maximum	Minimum	Average	MSE
X(mm)	6.9	5.0e-3	1.6	1.1
Y(mm)	6.0	8.0e-3	2.1	1.3
Z(mm)	3.6	4.0e-3	0.8	0.6

which consists of the validity and accuracy of the registration method, the accuracy of tracking, and the effectiveness of the foot tread interaction. The error between the position of the endoscope end and instrument tip is the critical measurement, which has three major components:

<1> The accuracy of the NDI measurement, although it has a precision of 0.02 mm.

<2> The accuracy of coordinate transformation between the NDI and UR Cartesian system.

<3> The accuracy of UR robot positioning accuracy, which has a precision of 0.1 mm. According to the above error, a tracking experiment without the virtual fixtures constraints is conducted by neglecting the effect of a missing NDI navigation signal. The result is shown in Fig. 10:

By considering the fixed 50Hz delaying frequency of the UR robot, error analysis of this tracking motion is as follows. Table 4 shows that the maximum error is approximately 8 mm because the error from the loss of the NDI navigation signal is also calculated. The average error is less than 3 mm, which meets the requirements of endoscopic sinus surgery.

To verify the effectiveness of the registration algorithm, the NDI navigation system is placed at different positions. Ten tracking experiments are conducted, and the 3D coordinate data of the instrument tip and endoscope end are recorded. The errors are shown in Fig. 11.

According to the built virtual fixtures and high precision of tracking motion, an experiment is performed to verify the validity of tracking based on VFs, which is shown in Fig. 12.

Finally, contrast tests are conducted by the same people in two different surgical modes: traditional endoscopic sinus surgery and RAESS based on our proposed automatic following motion with virtual constraints. The total surgical procedure is shown below, which was completed the "During the operation" process, and the operation process is omitted.

——Preoperative preparation: CT scan, open endoscope imaging system, disinfection and anaesthesia.

——During the operation: <1> Move the endoscope to the nasal turbinate while holding the dissection with the left hand and using turbinate scissors to observe the frontal entry with the right hand. <2> Adjust the robot (by foot pedal) to aim the endoscope at the opening; insert the secretions into the frontal sinus and aspirate the exudate. <3> Switch the right hand to forceps and open the frontal sinus to a 5 mm width and 10 mm height. <4> Adjust the robot (by foot pedal) to aim the endoscope at the front wall and cyst wall of the frontal sinus. Drain the cyst and diseased tissue using peeling forceps with the left hand.

——After the operation: Proper hemostasis, filling sponges or antibiotics.

The results show that the total time taken by the traditional mode is approximately 30 s, while the new model takes 50 s. Although a surgeon can operate with both hands to complete the test, the doctors are not familiar with the pedal control and tracking mechanism, which is related to the control strategy, and once the contact force exceeds the threshold force, the robot will automatically stop. Our proposed method is efficient, safe and practical, and it will save time with more operating experience. Our research promotes the development of RAESS and provides a technological innovation and breakthrough for the further realization of clinical and commercial uses of the nasal endoscope assisted robot.

VI. CONCLUSION

In this paper, to overcome the defects of motion control and safety protection in traditional RAESS, a new security motion control model for different nasal cavity shapes is proposed

and a forbidden virtual fixture based on a hyperbolic model is designed. The proposed method effectively constrains the spatial position of the robot, and the velocity constrains the spatial position, velocity, and behaviour of the robot. To completely free the doctor's hands, we design a tracking motion control strategy based on the mixed constraints of the proposed virtual fixtures and the safe threshold force model.

The experimental results show that the virtual fixture and control security models can effectively prevent collisions between surgical instruments and nasal tissue, effectively constrain the movement of the robot and can perform the operation task quickly and efficiently. The ultimate goal of our research is to make this method available for minimally invasive surgery. In the future, the combination of CT data and a hyperbolic model to create a new forbidden virtual fixture and path planning based on a guided virtual fixture is taken into consideration, and more automatic tracking patterns based on VFs to adjust different tasks should be created.

REFERENCES

[1] M. E. Wigand, "Transnasal ethmoidectomy under endoscopical control," *Rhinology*, vol. 19, no. 1, pp. 7–15, 1981.

[2] H. Stammberger, "Personal endoscopic operative technic for the lateral nasal wall—An endoscopic surgery concept in the treatment of inflammatory diseases of the paranasal sinuses," *Laryngologie, Rhinologie, Otologie*, vol. 64, no. 11, pp. 559–566, 1985.

[3] P. Castelnuovo, L. Dallan, P. Battaglia, and M. Bignami, "Endoscopic endonasal skull base surgery: Past, present and future," *Eur. Arch. Oto-Rhino-Laryngol.*, vol. 267, no. 5, pp. 649–663, 2010.

[4] C.-A. O. Nathan, V. Chakradeo, K. Malhotra, H. D'Agostino, and R. Patwardhan, "The voice-controlled robotic assist scope holder AESOP for the endoscopic approach to the sella," *Skull Base*, vol. 16, no. 3, pp. 123–131, 2006.

[5] S. E. Butner and M. Ghodoussi, "A real-time system for tele-surgery," in *Proc. 21st Int. Conf. Distrib. Comput. Syst.*, Apr. 2001, pp. 236–243.

[6] J. Marescaux *et al.*, "Transatlantic robot-assisted telesurgery," *Nature.*, vol. 413, no. 6854, pp. 379–380, 2001.

[7] M. O. Schurr, A. Arezzo, and G. F. Buess, "Robotics and systems technology for advanced endoscopic procedures: Experiences in general surgery," *Eur. J. Cardio-Thoracic Surg.*, vol. 16, pp. S97–S105, Nov. 1999.

[8] S. Aiono, J. M. Gilbert, B. Soin, P. A. Finlay, and A. Gordan, "Controlled trial of the introduction of a robotic camera assistant (endo assist) for laparoscopic cholecystectomy," *Surgical Endoscopy Other Interventional Techn.*, vol. 16, no. 9, pp. 1267–1270, 2002.

[9] P. Li *et al.*, "Development of a robotic endoscope holder for nasal surgery," in *Proc. IEEE Int. Conf. Inf. Automat. (ICIA)*, Aug. 2013, pp. 1194–1199.

[10] X. Dai *et al.*, "An endoscope holder with automatic tracking feature for nasal surgery," in *Proc. IEEE Int. Conf. Inf. Automat. (ICIA)*, Aug. 2016, pp. 1–6.

[11] Z. Zeng, Y. He, Q. Zhang, Y. Hu, and Y. Cao, "Approach and control for robot assisted sinus surgery," in *Proc. IEEE Int. Conf. Robot. Biomimetics (ROBIO)*, Dec. 2017, pp. 983–988.

[12] S. Park, R. D. Howe, and D. F. Torchiana, "Virtual fixtures for robotic cardiac surgery," in *Proc. Int. Conf. Med. Image Comput. Comput.-Assist. Intervent.* Berlin, Germany: Springer, 2001, pp. 1419–1420.

[13] A. M. Okamura, "Methods for haptic feedback in teleoperated robot-assisted surgery," *Ind. Robot, Int. J.*, vol. 31, no. 6, pp. 499–508, 2004.

[14] M. Li, M. Ishii, and R. H. Taylor, "Spatial motion constraints using virtual fixtures generated by anatomy," *IEEE Trans. Robot.*, vol. 23, no. 1, pp. 4–19, Feb. 2007.

[15] J. Ren, R. V. Patel, K. A. McIsaac, G. Guiraudon, and T. M. Peters, "Dynamic 3-D virtual fixtures for minimally invasive beating heart procedures," *IEEE Trans. Med. Imag.*, vol. 27, no. 8, pp. 1061–1070, Aug. 2008.

[16] J. Wurm, H. Steinhart, and K. Bumm, "A novel robot system for fully automated paranasal sinus surgery," *Int. Congr. Ser.*, vol. 1256, pp. 633–638, Jun. 2003.

[17] G. Strauss, K. Koulechov, R. Richter, A. Dietz, C. Trantakis, and T. Lüth, "Navigated control in functional endoscopic sinus surgery," *Int. J. Med. Robot. Comput. Assist. Surg.*, vol. 1, no. 3, pp. 31–41, 2005.

[18] K. Koulechov, G. Strauss, and R. Richter, "Mechatronical assistance for paranasal sinus surgery," *Int. Congr. Ser.*, vol. 1281, p. 636, May 2005.

[19] K. Koulechov, G. Strauss, A. Diets, M. Strauss, M. Hofer, and T. C. Lueth, "FESS control: Realization and evaluation of navigated control for functional endoscopic sinus surgery," *Comput. Aided Surg.*, vol. 11, no. 3, pp. 147–159, 2006.

[20] F. Rydén and H. J. Chizeck, "Forbidden-region virtual fixtures from streaming point clouds: Remotely touching and protecting a beating heart," in *Proc. IEEE/RSJ Int. Conf. Intell. Robots Syst. (IROS)*, Oct. 2012, pp. 3308–3313.

[21] B. C. Becker, R. A. MacLachlan, G. D. Hager, and C. N. Riviere, "Hand-held micromanipulation with vision-based virtual fixtures," in *Proc. IEEE Int. Conf. Robot. Automat.*, May 2011, pp. 4127–4132.

[22] M. Selvaggio, G. Notomista, F. Chen, B. Gao, F. Trapani, and D. Caldwell, "Enhancing bilateral teleoperation using camera-based online virtual fixtures generation," in *Proc. IEEE/RSJ Int. Conf. Intell. Robots Syst. (IROS)*, Oct. 2016, pp. 1483–1488.

[23] A. Nakazawa *et al.*, "Feedback methods for collision avoidance using virtual fixtures for robotic neurosurgery in deep and narrow spaces," in *Proc. 6th IEEE Int. Conf. Biomed. Robot. Biomechatron. (BioRob)*, Jun. 2016, pp. 247–252.

[24] A. Tang, Q. Cao, and T. Pan, "Spatial motion constraints for a minimally invasive surgical robot using customizable virtual fixtures," *Int. J. Med. Robot. Comput. Assist. Surg.*, vol. 10, no. 4, pp. 447–460, 2014.

[25] R. Fardel, M. Nagel, F. Nüesch, T. Lippert, and A. Wokaun, "Fabrication of organic light-emitting diode pixels by laser-assisted forward transfer," *Appl. Phys. Lett.*, vol. 91, no. 6, Aug. 2007, Art. no. 061103.

[26] J. Zhang and N. Tansu, "Optical gain and laser characteristics of InGaN quantum wells on ternary InGaN substrates," *IEEE Photon. J.*, vol. 5, no. 2, Apr. 2013, Art. no. 2600111.

QINGWEN ZHENG received the B.S. degree from Xiamen University, Xiamen, China, in 2016. He is currently pursuing the M.S. degree with the Harbin Institute of Technology, Shenzhen, China.

He has been performing a research as a Guest M.S. Student with the Shenzhen Institute of Advanced Technology, Chinese Academy of Sciences, since 2017. His research interests include surgical robots and interactive control and safety control algorithms.

YUCHENG HE received the B.S. degree from Southeast University, Nanjing, China, in 2004, and the M.S. degree from Xi'an Jiaotong University, Xi'an, China, in 2007.

He is currently a Research Assistant with the Center for Cognitive Technology, Shenzhen Institute of Advanced Technology, Chinese Academy of Sciences, China. His current research interests include medical assistant robots.

XIAOZHI QI received the B.S. degree from Yanshan University, in 2009, and the M.S. and Ph.D. degrees from the Harbin Institute of Technology, Shenzhen, China, in 2011 and 2017, respectively.

He is currently a Post-Doctoral Researcher with the Center for Cognitive Technology, Shenzhen Institute of Advanced Technology, Chinese Academy of Sciences, China. His current research interests include medical assistant robots and space deployable mechanisms.

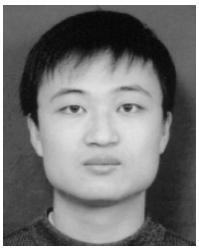

PENG ZHANG received the B.S. degree from Jilin University in 2003, and the M.S. and Ph.D. degrees from the School of Mechatronics Engineering, Harbin Institute of Technology, in 2005 and 2010, respectively.

He is currently a Senior Engineer with the Center for Cognitive Technology, Shenzhen Institute of Advanced Technology, Chinese Academy of Sciences, China. His current research interests include medical/surgical robots, medical automation equipment, and virtual simulation technology.

YING HU (M'11) received the B.S. degree from Shanghai Jiaotong University, Shanghai, China, in 1996, and the M.S. and Ph.D. degrees in mechanical engineering from the Harbin Institute of Technology, Shenzhen, China, in 1998 and 2007, respectively.

She is currently a Professor with the Center for Cognitive Technology, Shenzhen Institute of Advanced Technology, Chinese Academy of Sciences, China. She has authored or coauthored over 60 scientific papers published in refereed journals and conference proceedings. Her research interests include parallel robots, medical assistant robots, and mobile robots.

Bing Li (SM'16) received the Ph.D. degree from The Hong Kong Polytechnic University, Hong Kong, in 2001. He was a Professor of mechatronics in 2006.

He is currently the Head of the School of Mechanical Engineering and Automation, Harbin Institute of Technology, Shenzhen, China. His research interests include parallel manipulators and control, mechanical vibration and control.

Dr. Li is serving as an Associate Editor of the *International Journal of Mechanisms and Robotic Systems*.